

Self-Sensing Magnetic Bearings Using Parameter Estimation

Myounggyu D. Noh, Research Associate
Eric H. Maslen, Assistant Professor *

Abstract

A signal processing technique is presented by which the position of a rotor supported in magnetic bearings may be deduced from the bearing current waveform. The bearing currents are presumed to be developed with a two state switching amplifier which produces a substantial high frequency switching ripple. This ripple is demodulated using a model reference parameter estimation technique which extracts the length of the bearing air gap while rejecting the influence of amplifier voltage and duty cycle variation. The performance of the estimator is evaluated both by simulation and experiment. The method is demonstrated to produce a fairly wide bandwidth sensor with acceptably low feed-through of the bearing force.

1 Introduction

Active magnetic bearings require control based on feedback of the position of the suspended object. This feedback is required in order to achieve stability [1], but more importantly, in order to permit tailoring of the bearing dynamics to achieve targeted system performance [2]. Most magnetic bearing applications use feedback of the position along each axis of magnetic control.

Many potential applications of magnetic bearings require minimization of the number of wires which pass between the bearing controller and the magnetic components in the machine. Such a requirement may arise either from economic or reliability considerations. An exaggerated example is provided by the application of magnetic bearings to heart pumps [3, 4, 5] where wires must either pass through the chest cavity (transcutaneous) or be inductively coupled to an external transmission/reception device. In either case, minimizing the wire count is a paramount design concern.

The wires feeding the electromagnets can be minimized by interconnection of the magnets. A more substantial reduction in wire count can be achieved by eliminating the discrete position sensing devices and, instead, extracting an equivalent signal from information available in the electromagnet currents and voltages. This has the added benefit of removing most of the cost and potential failure of the sensor. Other potential advantages include elimination of sensor-actuator noncollocation [6] and reduction in amplifier switching noise infiltration.

Magnetic bearings which extract the position information from the electromagnet signals are referred to as “self-sensing”. Fundamentally, the sensing mechanism is the same as for a variable reluctance magnetic sensor [7] because the excitation frequency is generally too low to make significant use of eddy current effects.

The drawback to any self-sensing approach is that the design objectives in constructing the actuator are contrary to those in constructing a sensor. Capacity and thermal considerations usually lead to an actuator structure with magnetic paths whose reluctance substantially exceeds that of the air gaps at high frequencies (20 kHz or more). In contrast, high sensitivity and good rejection of magnetic nonlinearities are achieved in variable reluctance sensors by ensuring that the iron reluctance is on par with or substantially less than that of the air gaps. Thus, the overall sensing performance of a self-sensing magnetic bearing can be expected to be inferior to that of a discrete variable reluctance sensor when evaluated in terms of sensitivity, bandwidth, and linearity. The system-level advantages of self-sensing bearings must be weighed against expected performance shortcomings in deciding whether such an approach is appropriate to a given application.

Self-sensing magnetic bearings have been investigated extensively in the past ten years. The efforts can be grouped into two broad categories which differentiate the underlying theoretical approach. One category is parameter estimation where the bearing air gap is treated as a time varying parameter of an

*Authors are with the Department of Mechanical, Aerospace, and Nuclear Engineering, University of Virginia, Charlottesville, VA 22903, USA

isolated dynamic magnetic system – the bearing and amplifier combination. The present work falls into this category. The other approach is to treat the magnetic bearings and the supported object as a whole in which case the position of the supported object is not a parameter but a state.

Okada [8] reported a self-sensing magnetic bearing using a demodulation technique similar to the filter described in Section 5. Since the gap displacement modulates the amplitude of the switching waveform, the switching frequency component of the current is a direct indication of displacement. A serious drawback of the approach is that the estimation is also sensitive to the duty cycle of the PWM switching amplifier. The resulting force feed-through degrades the sensor performance. The present work specifically addresses this issue.

Mizuno, Bleuler, and Vischer [9, 10, 11] used a linear state-space observer to estimate the gap displacement. Treating the magnetic bearing as a two-port system, the linearized state-space equation describing the system is observable as well as controllable, making it possible to design a stable observer for the given system. Although it is stable, the resulting controller/observer pair usually has poor robustness [12]: small parameter variations in the physical system may produce instability.

In this work, a nonlinear parameter estimation technique is developed to estimate the position. A signal processing filter is designed to demodulate the switching waveform. The output of the filter is essentially a function of gap displacement, power supply voltage, and duty cycle. Rejection of force feed-through (duty cycle change) is achieved by implementing a parallel simulation of a gap dependent inductor model whose output is filtered in the same manner as the current waveform of the actual bearing. The error between the two demodulated waveforms is used to correct the gap estimate, thereby achieving displacement tracking.

2 System Model

Consider an eight-pole magnetic bearing shown in Figure 1. In the present work, we restrict our attention to estimation of the vertical position, indicated as x , through evaluation of the impedance of the two top coils: the lateral displacement of the rotor is assumed zero. The model presented here is readily extended to the problem of the fully coupled stator with both x - and y - displacements.

Following the usual magnetic circuit analysis [13] which assumes that

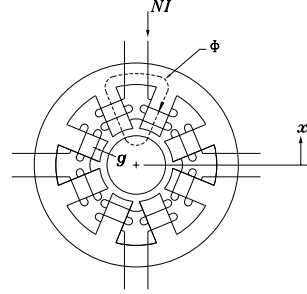


Figure 1: 8-pole magnetic bearing

- the magnetic material is linear
- gap flux density is uniform
- leakage flux is negligible
- the two coils wound on the top legs are wired in reverse series
- air gap length is small compared to gap arc length or axial length

the voltage across the top coil pair is derived from Ohm's and Faraday's laws:

$$V = N \frac{d\Phi}{dt} + IR \quad (1)$$

to yield the governing differential equation

$$\frac{di}{dt} = \frac{2(g - x \cos \theta) + l_c / \mu_r}{\mu_o N^2 A_g} \left(V - Ri - i \frac{dL}{dt} \right) \quad (2)$$

in which g is the nominal gap, θ is the angle between the pole leg centerline and the vertical, l_c is the effective iron length (taken along a mean flux path), μ_r is the relative permeability of the magnet iron, N is the number of coil turns in the two coils, A_g is the gap area, R is the total coil resistance, and L is the total coil inductance.

The voltage V in (2) switches very rapidly (35 kHz switching frequency in our experiments) between $-V_s$ and $+V_s$: a two state switching amplifier drives the coil. In the sequel, the term $i dL/dt$ in (2) is neglected because it is small compared to $V - iR$ when a switching amplifier is used. The duty cycle, α , of the amplifier is defined as the ratio of the time the amplifier applies the positive voltage to the total switching interval. Given this excitation, (2) describes a current waveform with a high frequency ripple whose amplitude is proportional to the position of the shaft, x . Therefore, amplitude demodulation will extract a signal which is proportional to x . However, since the amplitude is a function of the duty cycle and power

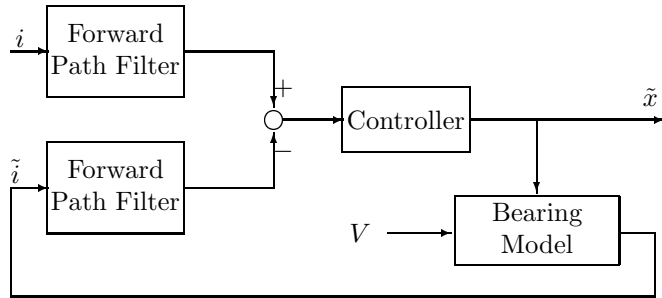


Figure 2: Overall schematic of the estimator

supply voltage as well as the gap, a mechanism is needed to reject the duty cycle in order to estimate the displacement without the substantial force feed-through.

3 General Approach

The air gap length ($g - x \cos \theta$) can be estimated in the following manner, as indicated in Figure 3. The measured current waveform is filtered to extract the amplitude of the switching component. At the same time, a real time simulation of the gap dependent coil inductance is supplied with the actual coil voltage V and an *assumed value*, \tilde{x} , of the air gap.

$$\frac{d\tilde{i}}{dt} = \frac{2(g - \tilde{x} \cos \theta) + l_c / \mu_r}{\mu_o N^2 A_g} (V - R\tilde{i}) \quad (3)$$

The resulting simulated switching waveform is filtered in the same manner as the measured waveform and the demodulated amplitudes are compared. The error (which is linear in the gap estimate error) is used to update the estimated air gap.

4 Experimental Setup

A test rig was designed to verify the proposed parameter estimator. The journal is supported by a beam which has greater compliance in the vertical direction than in the horizontal direction. This compliance prevents instability caused by the negative stiffness of the magnetic bearing. The bearing has an 8-pole design, schematically similar to the one shown in Figure 1. Table 1 lists the several critical values of the bearing. Two toggle clamps can be positioned at various points along the beam on each side of the bearing. By controlling the clamping location, various structural resonant frequencies can be obtained.

Coil turns, N	138
Nominal air gap, g_0	0.508 mm
Pole face area, A_g	99.68 mm ²
Iron core length, l_c	79 mm
Nominal inductance, L_0	2.35 mH

Table 1: Critical bearing parameters

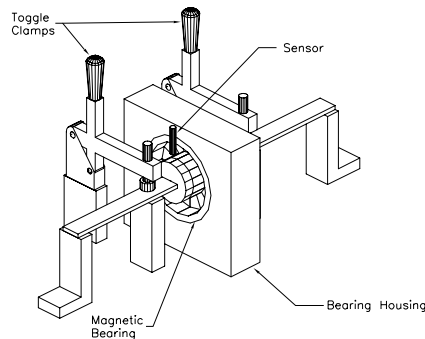


Figure 3: Sketch of the experimental setup

While injecting constant biases into the top and bottom coils, the beam is hit by a hammer to induce a free vibration. A sinusoidal coil current can be requested through the bearing amplifier for a forced vibration. The motion of the journal is measured with an eddy current type position probe as a reference signal. Figure 3 is a sketch of the test setup.

5 Forward Path Filter

The forward path filter demodulates the switching waveform and filters out the signal which is a function of duty cycle, power supply voltage, and gap length. Simulation and experimental results show that the forward path filter alone is inadequate to obtain reliable gap information because of filter nonideality, duty cycle variation, and switching nonideality.

5.1 Idealized Analysis

The objective of the forward path filter is to measure the amplitude of the switching waveform. Assuming that the waveform consists of low frequency components directly indicative of bearing force combined with a high frequency switching waveform, the first step in extracting the switching waveform is to apply a high pass filter. This filter should block all frequencies lower than the lowest frequency component

in the expected switching waveform and pass the remaining components unmodified. The amplitude of the resulting waveform can be measured by rectifying the signal and then averaging over some time scale, ideally a multiple of the switching waveform period. Such averaging is the behavior of an ideal low pass filter which blocks all frequencies higher than the inverse of the selected time scale.

Assuming a fixed-end PWM switching amplifier is used, the voltage applied to the inductor during one switching interval is described by

$$V(t) = \begin{cases} V_s, & 0 < t < \alpha\tau \\ -V_s, & \alpha\tau < t < \tau \end{cases} \quad (4)$$

where α is the duty cycle of the switching cycle. By integrating (3) with the voltage given in (4), the time history of current switching waveform is obtained as

$$i(t) = \begin{cases} I_0 + \frac{V_s}{L}t, & 0 < t < \alpha\tau \\ I_0 + \frac{V_s}{L}(2\alpha\tau - t), & \alpha\tau < t < \tau \end{cases} \quad (5)$$

In (5), the terms due to the resistance of the coil and back EMF are neglected. Since switching occurs at a high frequency (generally 20–50 kHz), it is reasonable to assume that the low frequency components of the signal vary linearly with time during one cycle. Therefore, the signal after an ideal high-pass filter is just the switching waveform minus the linear component of the current.

$$i_{HP}(t) = i(t) - \left[I_0 + (1 - 2\alpha)\beta V_s \left(\frac{t}{\tau} \right) \right] \quad (6)$$

Applying a full-wave rectifier and a low-pass filter results in a signal nearly equal to the average value of the switching waveform over one switching cycle. Figure 5.1 shows how the signal changes after each element in the filter. Assuming the low-pass filter is perfect, the output of the forward path filter is

$$u = \frac{1}{\tau} \int_0^\tau |i_{HP}(t)| dt \quad (7)$$

$$= \frac{1}{2}\alpha(1 - \alpha) \frac{V_s\tau}{\mu_o N^2 A_g} \left(g - x \cos \theta + \frac{l_c}{2\mu_r} \right)$$

This shows that the output signal is linearly dependent on the gap and power supply voltage, whereas it depends quadratically upon the duty cycle. This fact was demonstrated by Okada [8], whose approach is similar to the forward path filter described in this paper. As mentioned previously, the switching waveform is an amplitude-modulated signal which carries

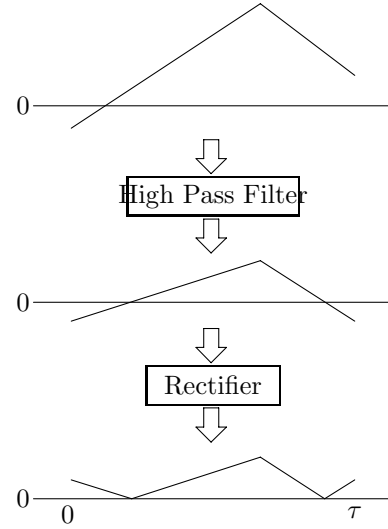


Figure 4: Representation of the signal at each processing point in the forward path filter.

gap information on its amplitude. Intuitively, therefore, demodulation of the switching waveform will result in the gap signal. However, as can be seen in (8), the demodulated signal is also quadratic in the duty cycle.

In principle, position estimation also can be done by measuring the duty cycle and rescaling the output of the forward path filter accordingly. This scaling approach, however, has several drawbacks such as the requirement of division, difficulty in measuring the duty cycle, and strong sensitivity to the real characteristics of the forward path filter.

5.2 Filter components

Several issues on implementing the forward path filter deserve attention. The forward path filter consists of a high pass filter, a fullwave rectifier, and a low pass filter. Each component is realized with analog integrated circuits.

High-pass filter: Experimentally, a state-variable filter [14] was used to realize the high-pass filter. The passband of the filter is chosen so that only the frequency components close to switching will pass through the filter. In actual realization, the cut-off frequency of the high-pass filter is set at about 10 % of the switching frequency; in this case, 4.46 kHz. The damping factor of the filter is close to 0.707 in order to achieve a maximally flat passband.

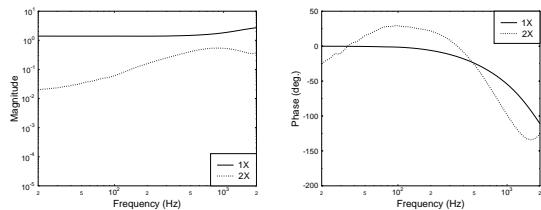


Figure 5: Frequency response of forward path filter (magnitude and phase)

Full-wave rectifier: There are several ways to realize an active full-wave rectifier [15]. The input signal to the rectifier should be adequate in magnitude so that the output of the rectifier not only maintains good signal to noise ratio but also does not exceed the slew rate limitation of the operational amplifier used to implement the rectifier.

Low pass filter: The same state-variable filter that was selected for implementing the high-pass filter was used for the low-pass filter. The cut-off frequency of the filter directly determines the bandwidth of the forward path filter and is limited by that of the high-pass filter. For the experimental work reported here, a cut-off frequency of 1.75 kHz was selected. The damping factor is again set at 0.707 to obtain a maximally flat passband with minimum phase distortion.

5.3 Performance of FP filter

Figure 5 shows the frequency spectrum of the forward path filter, which is obtained by computer simulation. Since the filter is nonlinear, the frequency response is valid only for the magnitude of the given input displacement amplitude (50 μm , in this case). One important result to note is that the second harmonic becomes significant above 500 Hz, as the output of the filter is quadratic in the duty cycle. Deviation of the actual filter performance from the idealized analysis is shown in Figure 6. The offset starts to increase rapidly above 500 Hz. When the duty cycle is fixed, the forward path filter performs reasonably well, as verified by an experiment shown in Figure 7 which compares the forward path filter output (solid line) to the actual journal motion as measured by a Bently Nevada eddy current proximator. It is clear from Figure 8, however, that the performance of the forward path filter degrades significantly if the duty cycle is changing over time.

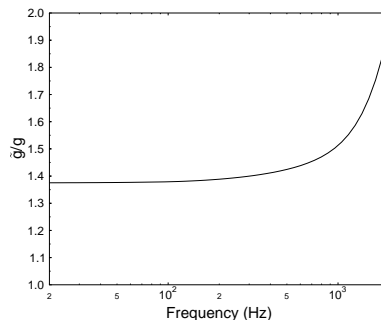


Figure 6: Ratio of offset to nominal gap

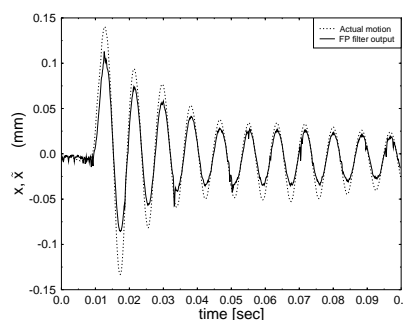


Figure 7: Performance of FP filter when the duty cycle is fixed

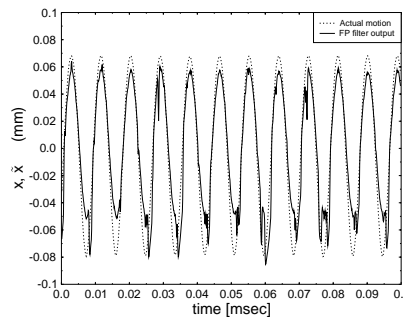


Figure 8: Performance of FP filter when the duty cycle is time-varying

6 Parameter Estimation

As described in Section 3, the estimator studied in this work employs a real-time simulation of the magnetic bearing inductance whose output is compared to the actual switching waveform: the error will correct the model. The approach herein is similar to a parameter servo system [16].

6.1 Idealization

The real-time simulation of the bearing inductance is based on the model described in Section 2 so the equation governing the simulation can be written as (3). If the simulated current passes through the same forward path filter as the actual current signal, the output of the filter is

$$\tilde{u} = \frac{1}{2}\alpha(1 - \alpha)\frac{V_s\tau}{gL_0}(g - \tilde{x} \cos \theta) \quad (8)$$

The error between the two outputs of the filter is a function of the duty cycle and the estimation error:

$$e = u - \tilde{u} = \frac{1}{2}\alpha(1 - \alpha)\frac{V_s\tau}{gL_0}(x - \tilde{x}) \cos \theta \quad (9)$$

6.2 PI controller

The transfer function from the point where the gap estimate \tilde{x} is injected to the error e between the two demodulated waveforms is essentially linear with a time varying gain (due to duty cycle variation). The high frequency roll-off of this transfer function is controlled by the characteristics of the low pass filter which follows the rectifier. Given this model, a proportional – integral type controller is chosen to drive the error to zero because of simplicity and robustness. Stability of the closed loop (see Figure 3) was evaluated using Popov's circle criterion [17] (because of the time varying gain) and the loop gain adjusted to ensure an adequate gain margin while maximizing the closed loop bandwidth. The transfer function of the controller is

$$G_c(s) = \left(K_p + \frac{K_i}{T_i s + 1} \right) \left(\frac{\omega_{pi}}{s + \omega_{pi}} \right) \quad (10)$$

in which the parameters for the test circuit were chosen to be: $K_p = 0.0002$, $K_i = 0.1$, $T_i = 0.01$, and $\omega_{pi} = 1 \times 10^5$.

6.3 Performance of the Parameter Estimator

Figure 9 shows the frequency response of the pa-

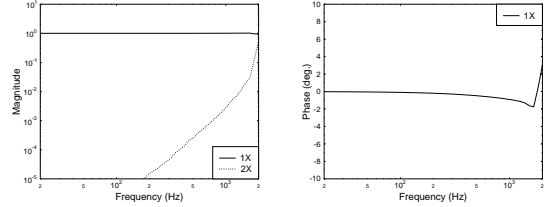


Figure 9: Frequency response of parameter estimator (magnitude and phase)

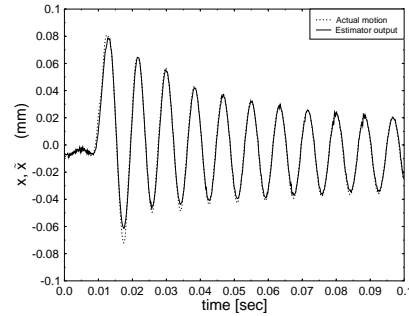


Figure 10: Performance of parameter estimator when the duty cycle is fixed

parameter estimator obtained from computer simulation with the same operating conditions as in Figure 5. The harmonic components are reduced considerably and the phase lag up to 1 kHz is insignificant. Experimental results also verify the improvement made by the introduction of the parameter estimator. Figure 10 shows the estimator (solid line) tracking the actual displacement (dotted line), when the force in the bearing remains constant.

With a time-varying duty cycle, there is no noticeable performance degradation, as shown in Figure 11 where the force is time-varying with a mag-

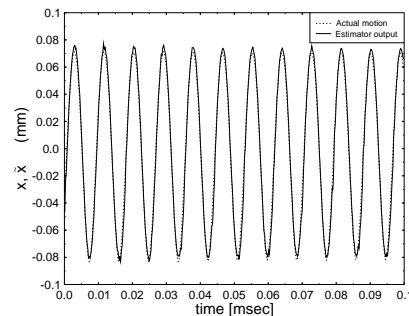


Figure 11: Performance of parameter estimator when the duty cycle is time-varying

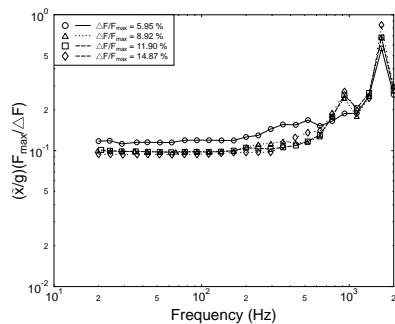


Figure 12: Estimation error due to duty cycle change

nitude of 3.6 % of the bearing load capacity. To quantize the effect of duty cycle change, a force feed-through test was done, where the beam is secured with the toggle clamps described earlier and sinusoidal forces with several different amplitudes are applied. The result of the test is shown in Figure 12. The force feed-through gain remains constant up to 500 Hz and starts to increase with frequency. The magnitude of the force fluctuation has little influence on the gain, which indicates the linearity of the force feed-through. In absolute terms, the estimator error due to force feed-through is about $5 \mu\text{m}$ (1 % of the nominal gap), when the force fluctuation is one tenth of the bearing load capacity. The force feed-through effect could be reduced by employing a higher order high-pass filter, with some resulting sacrifice of bandwidth.

7 Conclusions

Realization of a self-sensing magnetic bearing requires estimation of the gap position without employing separate position sensors. When a bi-state switching amplifier is driving a magnetic bearing coil, the switching noise of the current signal is modulated with a displacement signal, since the bearing is essentially a variable reluctance sensor. A filter is designed to demodulate the current signal. The forward path filter produces reliable position estimation only when the duty cycle of the amplifier is fixed. By the introduction of the simulated bearing model and a servo-controller for the inductance of the coil, the position estimation improves considerably in terms of accuracy and bandwidth.

8 Acknowledgements

This research was supported in part through a research grant from NASA's Lewis Research Center and in part by the University of Virginia Center for Magnetic Bearings which is funded by the Center for Innovative Technology of the Commonwealth of Virginia.

References

- [1] S. Earnshaw, "On the nature of molecular forces," *Transactions of the Cambridge Philosophical Society*, vol. 7, pp. 97–112, 1842.
- [2] R. R. Humphris, R. D. Kelm, D. W. Lewis, and P. E. Allaire, "Effect of control algorithms on magnetic journal bearings," *Trans. ASME Journal of Engineering for Gas Turbines and Power*, vol. 108, pp. 624–632, October 1986.
- [3] T. Akamatsu *et al.*, "Centrifugal blood pump with magnetically suspended impeller," *Artificial Organs*, vol. 16, no. 3, 1992.
- [4] G. Bramm and D. B. Olsen, *Seal and Bearingless Rotary Blood System*. Springer-Verlag, 3rd ed., 1989.
- [5] D. B. Olsen and G. Bramm, "Blood pump with a magnetically suspended impeller," *Transactions of American Society for Artificial Internal Organs*, 1985.
- [6] V. A. Spector and H. Flashner, "Modeling and design implications of noncollocated control in flexible systems," *Journal of Dynamic Systems, Measurement, and Control*, vol. 112, pp. 186–193, June 1990.
- [7] R. L. Maresca, "A general method for designing low-temperature drift, high-bandwidth, variable-reluctance position sensors," *IEEE Transactions on Magnetics*, vol. 22, pp. 118–123, March 1986.
- [8] Y. Okada, K. Matsuda, and B. Nagai, "Sensorless magnetic levitation control by measuring the PWM carrier frequency component," in *Proceedings of the Third International Symposium on Magnetic Bearings*, 1992.
- [9] T. Mizuno, H. Bleuler, C. Gähler, and D. Vischer, "Towards practical applications of self-sensing magnetic bearings," in *Proceedings of the Third International Symposium on Magnetic Bearings*, 1992.

- [10] H. Bleuler, "A survey of magnetic levitation and magnetic bearing types," *JSME International Journal*, vol. 35, no. 3, pp. 335–342, 1992.
- [11] D. Vischer and H. Bleuler, "Self-sensing active magnetic levitation," *IEEE Transactions on Magnetics*, vol. 29, pp. 1276–1281, March 1993.
- [12] J. C. Doyle, "Guaranteed margins for LQG regulators," *IEEE Transactions on Automatic Control*, vol. AC-23, pp. 756–757, August 1978.
- [13] L. W. Matsch, *Electromagnetic & Electromechanical Machines*. Harper & Row, 1977.
- [14] Burr-Brown, *Burr-Brown IC Data Book*. 1995.
- [15] W. G. Jung, *IC Op-Amp Cookbook*. SAMS, 3rd ed., 1986.
- [16] J. E. Gibson, *Nonlinear Automatic Control*, ch. 11, pp. 491–547. McGraw-Hill, 1963.
- [17] H. K. Khalil, *Nonlinear Systems*. Macmillan Publishing Company, 1992.